Rifting of the Kalahari Craton Through Botswana? New Seismic Evidence

H. Paulssen[1] , T. Micallef[1,2] , D. R. Bouwman[1,3], E. Ruigrok[1,4] , M. W. Herman[1,5] , I. Fadel[6] , Mark van der Meijde[6] , M. Kwadiba[7], J. Maritinkole[7], and O. Ntibinyane[7,8]

[1]Department of Earth Sciences, Utrecht University, Utrecht, The Netherlands, [2]Now at Nestlé, Amstelveen, The Netherlands, [3]Now at Royal HaskoningDHV, Amersfoort, The Netherlands, [4]R&D Seismology and Acoustics, Royal Netherlands Meteorological Institute, De Bilt, The Netherlands, [5]Now at Department of Geological Sciences, California State University, Bakersfield, CA, USA, [6]Faculty of Geo-Information Science and Earth Observation, University of Twente, Enschede, The Netherlands, [7]Botswana Geoscience Institute, Lobatse, Botswana, [8]Now at Comprehensive Nuclear-Test-Ban Organization (CTBTO), Vienna, Austria

Abstract Botswana is a country with relatively low seismic activity that experienced an unexpected Mw 6.5 earthquake on 3 April 2017. Using data from the first countrywide seismic network, we established a Botswana earthquake catalog for the period January 2014 to February 2018. Two areas of elevated seismic activity were detected. The first one is the Okavango Rift Zone in northern Botswana, an area that is known to be active. The other one is associated with the 2017 mainshock and its aftershocks in central Botswana; it follows the Paleoproterozoic suture between the Limpopo Belt and the Kaapvaal Craton. Double-difference relocation of these events revealed a reactivated fault system with a northwesterly strike with the aftershocks occurring at shallower depths than the mainshock at 29 km. The focal mechanisms of the mainshock and selected aftershocks are of normal faulting type with strikes similar to the orientation of the fault system. The unidirectional rupture of the mainshock in the lower crust combined with the upward migration of the aftershocks along the Moiyabana Fault and a thin low velocity anomaly the uppermost mantle are consistent with the events being produced by eclogitization of a dry metastable granulite facies rock by fluid intrusion from the mantle in an extensional stress regime. The Okavango Rift Zone is generally interpreted as the terminus of the southwestern branch of the East African Rift System. We suggest that the recent earthquakes in central Botswana may be considered as the southern continuation of this branch.

Plain Language Summary Earthquakes do not happen very often in Botswana, but an unexpected magnitude 6.5 earthquake occurred on 3 April 2017. We investigated earthquake occurrence in Botswana for the period January 2014 to February 2018 using data from the first countrywide seismic network. We found that the magnitude 6.5 earthquake in central Botswana was located deep in the crust and that the aftershocks were all at shallower depths. The main- and aftershocks were located along the boundary between two cratonic blocks that were welded together 2.6 Gyr ago. The earthquakes show that this fault zone is now reactivated in a stress regime that leads to rifting. It is likely that the earthquakes are caused by fluid infiltration from the mantle into the crust, altering the rock of the ancient fault zone. It is generally thought that the seismically active Okavango Rift Zone in northern Botswana is the (southern) end of the southwestern branch of the (continental scale) East African Rift Zone. We suggest that this branch has progressed southwards through central Botswana.

1. Introduction

Botswana is a country characterized by low to moderate seismic activity. It has long been thought that most earthquakes occur in the north along the Okavango Rift Zone, the southwestern terminus of the East African Rift System (e.g., Leseane et al., 2015; Reeves, 1972). However, recent seismicity and geodetic studies (Nthaba et al., 2018; Pastier et al., 2017) and the occurrence of the 2017 Mw 6.5 earthquake in central Botswana indicate that other regions have greater seismic potential than previously thought. However, the detection and localization of earthquakes with small magnitude has long been hampered by the paucity of seismic stations in Botswana. This changed with the deployment of 21 broadband stations of the NARS-Botswana network in 2013 (Figure 1, https://seismologie.sites.uu.nl/research-projects/nars/botswana). The network was originally planned as a temporary

deployment, but in 2018 it was transformed to the permanent Botswana Seismological Network operated by the Botswana Institute of Geosciences (https://www.fdsn.org/networks/detail/BX).

In this study we used data of the NARS-Botswana network to build a 4-year catalog of seismic events in Botswana that, for the first time, includes reliable epicentral locations of low magnitude events (Section 3). With the double-difference method, we relocated the aftershocks of the 3 April 2017, central Botswana mainshock to identify the fault system that was active (Section 4). Focal mechanisms of several $M > 4$ events were determined by waveform modeling to infer a normal-faulting related extensional stress regime (Section 5). Using an empirical Green's function approach, we resolved the rupture propagation of the mainshock (Section 6). Together, the results of this study provide new insights into the processes that are associated with cratonic rifting in Botswana in an area that up to recently was considered aseismic (Section 7).

2. Tectonic Setting and Botswana Seismicity

The crustal structure of Botswana is dominated by Archean cratons that are surrounded by mobile belts which formed by successive periods of amalgamation and rifting (Begg et al., 2009; Key & Ayres, 2000). Figure 1 shows the main tectonic units, with the Zimbabwe Craton in the east and the Kaapvaal Craton in the south. During the Paleoproterozoic these two Archean cratons were welded together with the originally Archean Limpopo Belt caught in between, resulting in extensive deformation of the Limpopo Belt. Together, the three units form the Kalahari Craton. The southeastern edge of the Archean Congo Craton is located in the northwestern tip of Botswana. The nature of the Rehoboth Province in the southwest is still unclear, mainly because it is covered by more than 10 km of Paleozoic and younger sediments (Wright & Hall, 1990). The region has been interpreted as the western extension of the Kaapvaal Craton, but recent tomographic results by Ortiz et al. (2019) and Fadel et al. (2020) suggest that it is more likely a separate microcraton (Maltahohe).

The Magondi Belt, Okwa Block and Kheis Belt which surround the Kalahari Craton are all of Paleoproterozoic age. The boundaries of these regions are mainly inferred from magnetic and gravity data because most of the area is covered by a thick layer of sediments from the Kalahari desert. This sedimentary cover also hampers the localization of the boundary between the Limpopo and Magondi Belt (Chisenga et al., 2020). A northwest-southeast trending rift crosses central Botswana, with volcanic rocks of Mesoproterozoic age exposed along the Ghanzi Ridge and in the Chobe District (Key & Ayres, 2000). During the Neoproterozoic-Lower Paleozoic this Ghanzi-Chobe Rift was overprinted by an inland arm of the Damara Orogenic Belt.

The Okavango Rift Zone in northern Botswana comprises a number of northeasterly trending faults that are currently active. It is an incipient continental rift and is considered to be the terminus of the southwestern branch of the East African Rift System (e.g., Bufford et al., 2012; Kinabo et al., 2007; Leseane et al., 2015; Reeves, 1972; Scholz et al., 1976).

Whilst Botswana is a country with a low level of natural seismicity, moderate to large earthquakes were up to recently only associated with the Okavango Rift Zone. Between 1952 and 1953, 33 events occurred in the region, most of them with a magnitude greater than 5.0 and two of them with magnitude 6.1 and 6.7. Seismicity then declined: from 1954 to 1955 only two magnitude 5.0 events were observed in northern Botswana, and in the subsequent 10 years only three other minor events (Reeves, 1972). The reviewed ISC catalog only lists nine events between 1990 and 2014 with magnitudes ranging between 3.1 and 4.8 (ISC, 2018).

Whereas it is clear that Okavango Rift Zone is seismically active, some other active regions may well have remained undetected because of the very low number of seismic stations in the country, as was pointed out by Pastier et al. (2017) and Nthaba et al. (2018). The notion that there may be unknown regions with seismically active faults was confirmed by the occurrence of the recent Mw 6.5, 3 April 2017, earthquake in central Botswana. The earthquake was located in a region with low historical seismicity and far away from any hitherto identified active fault (Kolawole et al., 2017; Midzi et al., 2018).

Previous studies using the NARS-Botswana network focused on the crustal and upper mantle structure. Crustal thickness variations, inferred from receiver functions, were found to vary between 34 km for the Okavango Rift Zone to 49 km at the border between the Magondi Belt and Zimbabwe Craton (Fadel et al., 2018). Rayleigh wave tomographic studies showed high upper mantle shear wave velocities (4.7–4.8 km/s) beneath
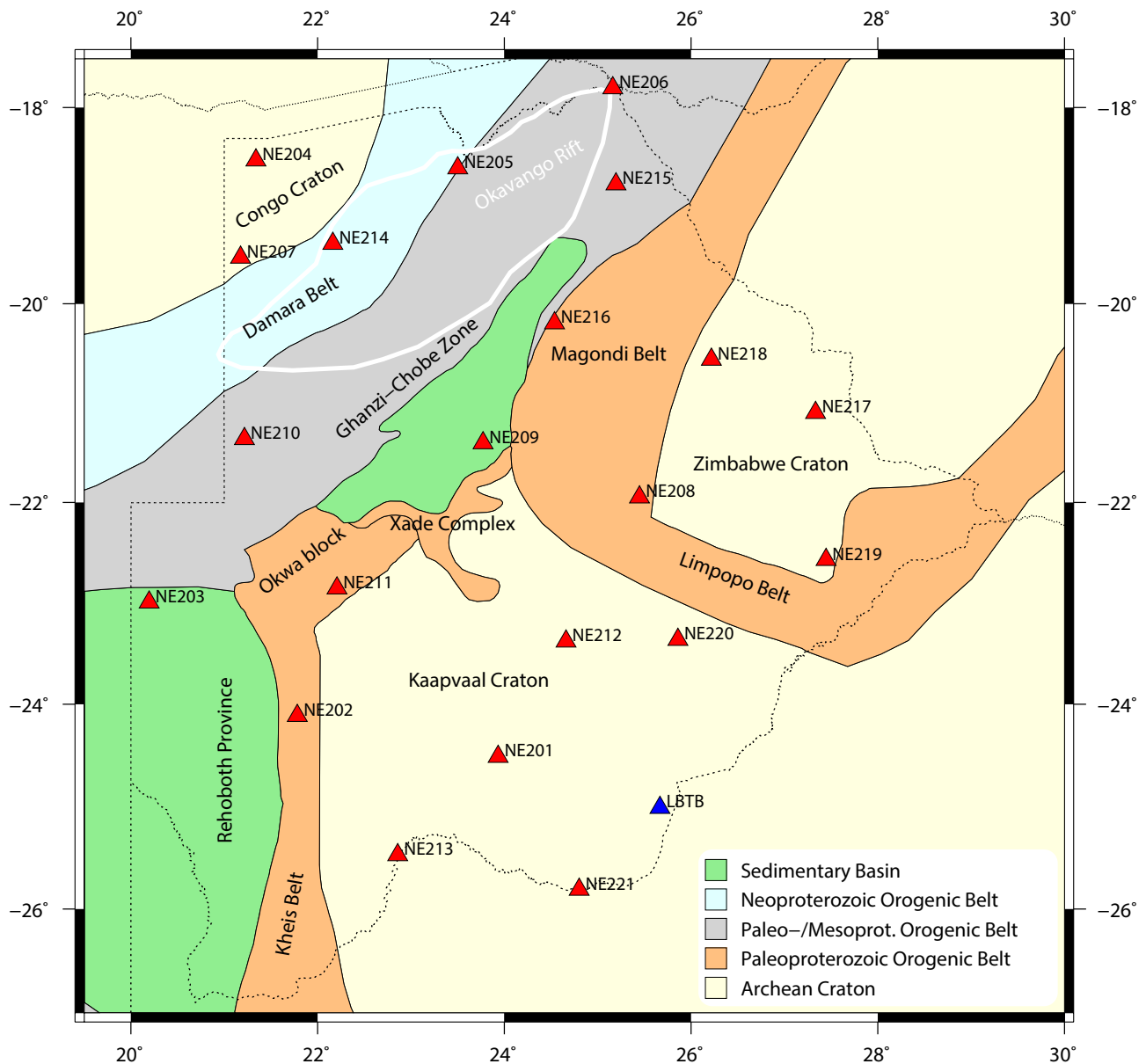
Figure 1. Major tectonic units of Botswana based on Fadel et al. (2020) and Leseane et al. (2015), NARS-Botswana stations (red triangles) and station LBTB (blue triangle).

the Kaapvaal, Zimbabwe and Congo cratons down to depths of 200–250 km, whereas low upper mantle shear velocities (4.4–4.5 km/s) were obtained beneath the northeastern part of the Okavango Rift Zone which are likely associated with the southwestern branch of the East African Rift System (Fadel et al., 2020; White-Gaynor et al., 2021).

In this study we investigate the Botswana seismicity by analysis of the continuous data of the NARS-Botswana network. We then improve the (relative) locations of the 2017 mainshock and its aftershocks using the double-difference method and determine the focal mechanisms of the seven largest events as well as the rupture propagation of the mainshock to better understand the nature of this intraplate seismicity.

3. Event Detection and Localization

We used the NARS-Botswana data for the period from 1 January 2014 to 28 February 2018 to obtain a Botswana event catalog that improves on other catalogs (which are mainly based on data from stations outside the country) both in terms of detection as well as localization of the epicenters. Because there are various mines in the country (Figure 2), not only tectonic earthquakes will be detected but also mining related events.

We employed the SeisComP3 software package (GFZ, 2008) with automatic and manually picked *P*-wave arrival times to detect and locate seismic events. The procedure is summarized as follows. First, a simple STA/LTA (short-term average/long-term average) detector was applied to the 0.7–2.0 Hz filtered data to obtain rough estimations of potential first *P*-wave arrivals. After event identification, that is, recognizing that multiple *P*-wave arrivals are associated to a single event, an AIC *P*-phase picker, based on the the Akaike Information Criterion (St-Onge, 2011), was applied to the 0.5–5 Hz filtered data to achieve more accurate arrival times. Finally, all automatically determined *P*-wave arrivals were manually reviewed and modified if necessary. To ensure that no seismic events were missed, the detected events by SeisComP3 were compared to the catalog of unreviewed events published by the ISC (ISC, 2018). Events that were not identified by SeisComP3 but that were listed by the ISC were used as potential additional events for which the data were analyzed. If sufficiently clear, new *P*-wave arrivals were manually picked for those events as well. In the last step, the picked *P*-wave onset times were used to locate the seismic events using the reference model iasp91 (Kennett & Engdahl, 1991). Events were located if at least six *P*-wave picks were available with a maximum individual residual of 7.0 s and a final root mean square (RMS) residual less than 3.5 s. The procedure, including all parameter settings, is described in detail in Micallef (2019). The final catalog consists of 376 Botswana events and includes magnitude estimates that are derived from the high-frequency *P*-wave amplitudes. The magnitude of completeness was estimated from the Gutenberg-Richter relationship for events prior to the 2017 mainshock (Micallef, 2019), giving a value of 3.1. The catalog is provided in Table T1 of Supporting Information S1.

A map of the events is presented in Figure 2. It shows two main regions of natural seismic activity: one in the Okavango Rift Zone in northern Botswana with magnitudes ranging from 3.0 to 4.9, and the other in central Botswana which includes the 3 April 2017, mainshock and its aftershocks. Note that many other seismic events are related to mining.

Within the Okavango Rift Zone, seismic activity was highest in the eastern part of the region for the period of investigation. This is also observed in the seismotectonic map by Meghraoui and the IGCP-601 Working Group (2016) who re-evaluated historical and instrumental earthquake catalogs of the African continent. The correspondence indicates that the elevated seismicity in the eastern Okavango Rift Zone is a real feature, not biased by the limited time span of our data. It is broadly believed that seismicity in the Okavango Rift Zone is caused by the development of an active rift, that is, to the continuation of the southwestern branch of the East African Rift System which enters Botswana in the northeast (Kinabo et al., 2007; Modisi et al., 2000; Scholz et al., 1976). Moreover, it has been suggested that the earthquakes in the Okavango Rift Zone are facilitated by ascending fluids from a hot mantle along lower-crustal faults. This is inferred from the thermal structure derived from aeromagnetic and gravity data (Leseane et al., 2015) as well as from the seismic structure obtained from surface wave tomography (Fadel et al., 2020). It is likely that the process of rifting and upward fluid transport from the mantle is further developed in the northeastern and eastern part of the Okavango Rift Zone (i.e., the terminus of the southwestern branch of the East African Rift System), which would explain the dominant seismicity at the eastern parts of the reactivated faults.

The other region of natural seismicity includes the 3 April 2017, Mw 6.5 earthquake in central Botswana at 120 km distance from the village of Moiyabana (Kolawole et al., 2017). The epicenter, located by our data at 22.636°S, 25.206°E, matches the location given by the International Seismological Center (ISC) within the uncertainties. It was the largest earthquake recorded by the network and was completely unexpected because it occurred in a region without major tectonic activity in the last ~2 Ga (Kolawole et al., 2017). Previous studies, not using NARS-Botswana data, showed that it was a normal faulting event along a northwest striking fault (Gardonio et al., 2018; Materna et al., 2019; Midzi et al., 2018), although the studies do not agree on the direction of fault dip.

The main event was followed by 216 aftershocks (up to 4 February 2018) which are clustered along a NW-SE trending zone (Figure 2). This matches the aftershock distribution for the month of April 2017 measured by a temporary network installed immediately after the mainshock (Midzi et al., 2018). Yet, our longer-term earthquake distribution extends further to the northwest, and clearly shows that the events cluster around the boundary between the Kaapvaal Craton and the Limpopo Belt (Figures 2 and 4b).

We carefully checked our catalog for the presence of potential foreshocks because the main event occurred in a remote area without any seismicity that was reliably detected. Two events, with magnitudes between 2 and 3, occurred at distances of ~40 km northwest of the main event (within the same zone as the aftershock seismicity) on 27 October 2014, and 10 March 2015. Although they are not true foreshocks in the sense that they occurred just before the main event, they do provide evidence for seismic activity along the boundary between the Kaapvaal Craton and the Limpopo Belt prior to the main event. Notably, even after careful data inspection, we
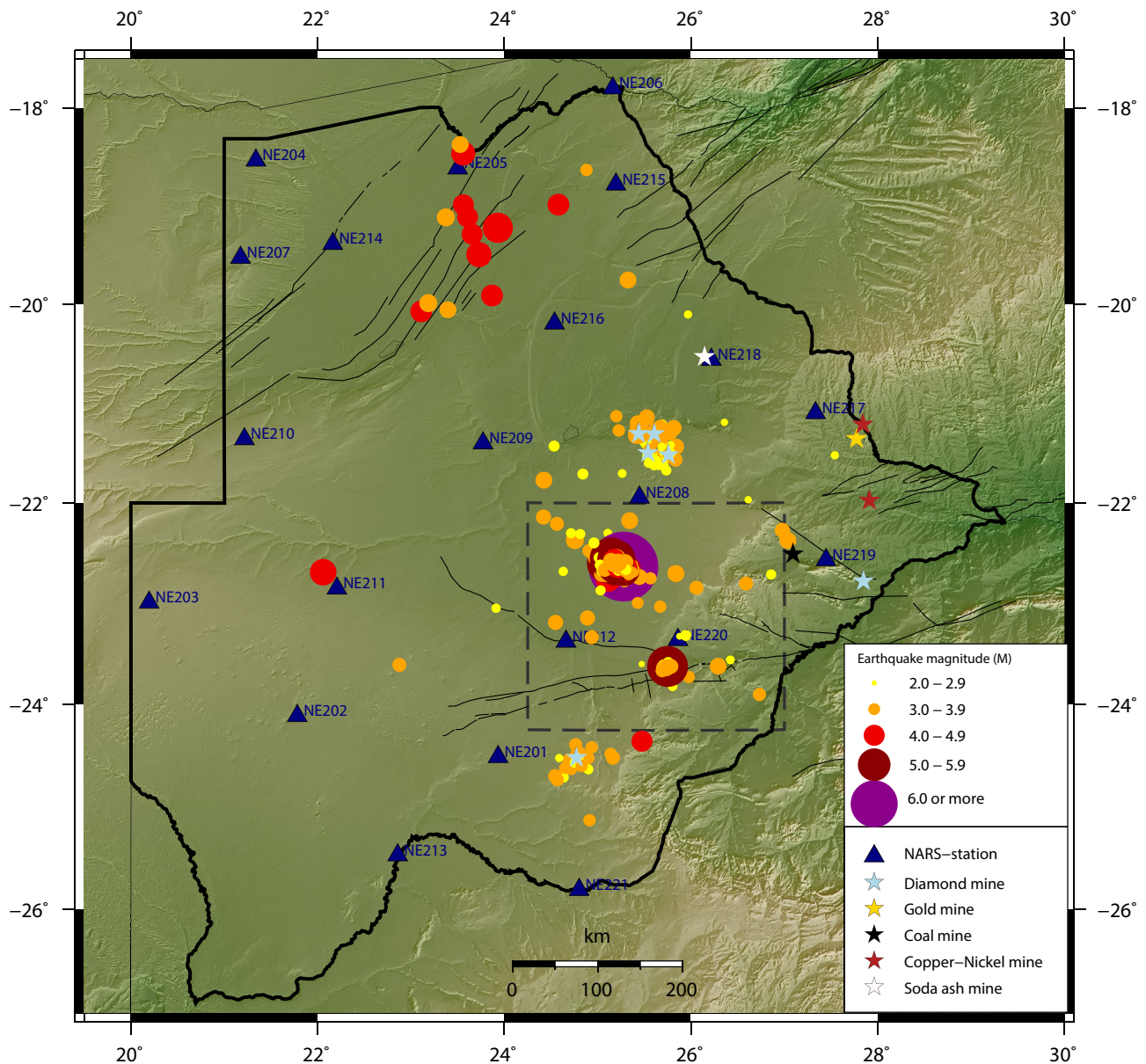

Figure 2. Epicenters of the seismic events. Faults, indicated by the thin black lines, are from Meghraoui and the IGCP-601 Working Group (2016). Mines are indicated by stars. The area within the dashed box is shown in Figure 3.

did not detect any of the 20 foreshocks with M > 3 identified by Gardonio et al. (2018), who applied a template matching technique to data recorded at distances larger than 1200 km from the main event.

On 12 August 2017, an earthquake with an estimated magnitude of 5.6 occurred at 23.626°S, 25.678°E. It is located within the Kaapvaal Craton, 120 km southeast of the main event, at the junction of the WSW-ENE trending Zoetfontein Fault with a southern branch and a northwesterly branch extending to central Botswana. The area is known to be seismically active, but mostly with magnitudes smaller than 5 (Meghraoui & the IGCP-601 Working Group, 2016). Several small events in our catalog can be associated to these known faults in the Zoetfontein Fault region of Kaapvaal Craton (Figure 2).

In addition to the tectonic events, a few clusters of mining events were detected (Figure 2). Most of them are from explosions in diamond mining areas (around 21.3°S, 25.5°E and 24.5°S, 24.7°E) and a few are related to coal mining (22.5°S, 27.0°E). Albano et al. (2017) verified that the 3 April 2017, main event was not caused by mining.

4. Relocation of the Aftershocks of the 3 April 2017, Earthquake

Aftershock distributions are useful to identify the fault plane and to determine the evolution of aftershock related fault slip. In an analysis that was carried out independently from the localization study presented in the previous section, we relocated the aftershocks of the 3 April 2017, earthquake with the double-difference method by Waldhauser and Ellsworth (2000). The double-difference method is based on the notion that the ray paths of two nearby events to the same station are similar along most of their ray paths if the hypocentral distance between the two events is small compared to (a) the event-station distance and (b) the scale length of velocity heterogeneity. If pairs of events meet these conditions, then their travel time differences observed at a common station can be attributed to the spatial offset between the events. This allows very accurate relocation of events with respect to each other if travel time differences of multiple stations with a good azimuthal distribution around the earthquake are used.

We relocated the 3 April 2017, mainshock together with 79 aftershocks with M ≥ 2.5 (until 9 November 2017) using the original locations from the ISC and USGS catalogs. *P*-wave arrival times were manually picked on seismograms of the NARS-Botwana network as well as of station LBTB of the Global Telemetered Seismograph Network. Relocation was done using the velocity structure at the location of the mainshock obtained from the tomographic model by Fadel et al. (2020). Tests were carried out on subsets of the data using various parameter settings and solving the system by either singular value decomposition (SVD) or the conjugate gradient algorithm LSQR (Paige & Saunders, 1982). Because of the number of events, the inversion of the entire data set was performed using LSQR and a full description of the parameter settings is given in Bouwman (2019).

Of the 80 events in total, 57 events were relocated in the area around the mainshock. Two events, the event in the Kaapvaal Craton on 12 August 2017, and an aftershock on the same day, were relocated as a separate cluster 113 km southeast from the mainshock. The other events could not be relocated because their initial locations were too far away from these two clusters. The relocated events were found to have mean two-sigma standard errors of ~4.5 km in the three orthogonal directions ($2\Delta x = 4.4$ km, $2\Delta y = 4.6$ km, $2\Delta z = 4.4$ km) with depth errors (Δz) ranging between 0.4 and 1.2 km. More accurate relative locations might be obtained by including *S*-wave arrivals, although they are harder to pick.

The results, presented in Figure 3 and as Table T2 in Supporting Information S1, show that the dispersed distribution of hypocenters around the mainshock becomes a 24-km long zone of aligned aftershocks. Notably, the aftershocks are all located northwest of the mainshock and decrease in depth in the northwest direction. The cross-section of Figure 3 shows that the hypocenters are relocated along a plane with a dip of ~70° toward the northeast. We observe that the main event is relocated at significantly shallower depth (18 km) compared to the original USGS location (29 km). This is caused by the fact that the double-difference method is a relative relocation method, keeping the center of the event distribution in place. With most of the aftershocks originally being located at the default depth of 10 km, whereas their actual depth is probably deeper (see next section), the relocated events are likely to be shifted upward compared to reality.
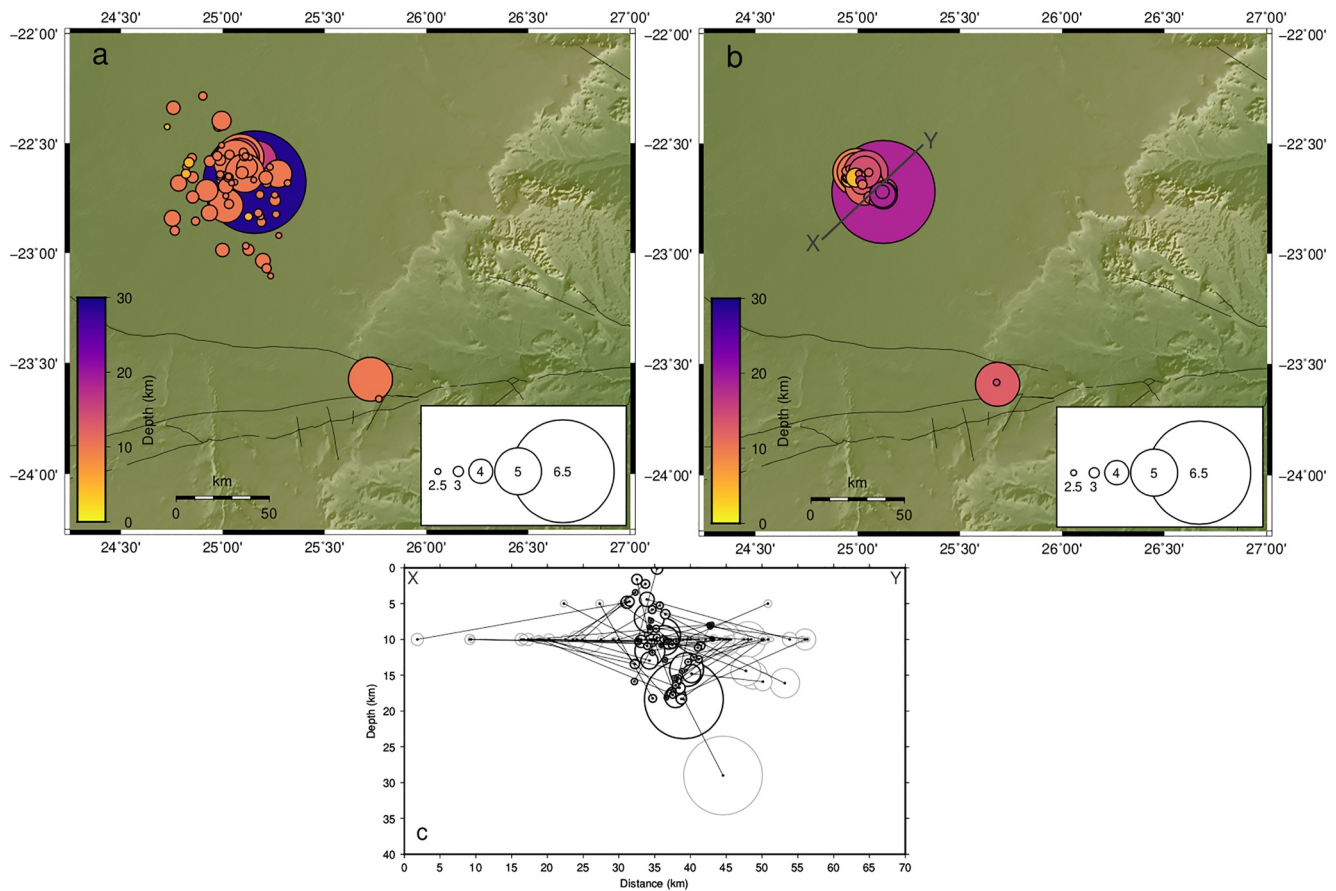
Figure 3. (a) Original and (b) relocated hypocenter locations in map view. (c) Original (gray) and relocated (black) events along cross-section X-Y indicated in (b).

5. Focal Mechanisms and Hypocenter Depths

The previous localization and relocalization studies only used first arrival times. On the other hand, *P* and *S* waveforms (including surface reflected phases such as *pP* and *sS*) constrain focal mechanism, depth and magnitude of earthquakes. We modeled the *P* and *S* waveforms with the "cut and paste" (CAP) method of Zhao and Helmberger (1994) (see also W. Chen et al., 2015; Zhu & Helmberger, 1996). Green's functions were calculated with the Thompson-Haskell propagator method, and the 1-D model to calculate the synthetics is based on the average Botswana mantle model by Fadel et al. (2020) combined with the crustal structure at the location of the mainshock from the same study. A grid search is performed to find the optimum source parameters (focal depth, moment magnitude and strike, dip, rake for a double-couple point source) using the L2 misfit between data and synthetics. The method allows for travel time shifts caused by 3-D heterogeneity that are not accounted for by the 1-D velocity model. The *P* waveforms were filtered between 0.05 and 0.3 Hz and the *S* waveforms between 0.05 and 0.2 Hz to minimize the influence of anthropogenic and microseismic noise.

We applied the method to events with M > 4 which had sufficient signal-to-noise ratio: the 3 April 2017, main event, five aftershocks in its immediate vicinity and the 12 August 2017, earthquake at the Zoetfontein Fault. Figure 5 illustrates the waveform fits for the 4 July aftershock. Figure 6 presents all results and they are also listed in Table 1.

The 3 April 2017, mainshock and its aftershocks are all normal faulting events with a NW-SE strike, a strike that is consistent with the aftershock distribution (Sections 3 and 4) and the orientation of the boundary between the Kaapvaal Craton and Limpopo Belt. The event at the Zoetfontein Fault has a similar mechanism, suggestive of extension perpendicular to NW-SE oriented faults in the entire area. Furthermore, we found that all events occurred at depths between 20 and 30 km, with the main event at 29 km being the deepest. The focal mechanism and event depth of the mainshock are similar to previous studies (Gardonio et al., 2018; Kolawole et al., 2017;
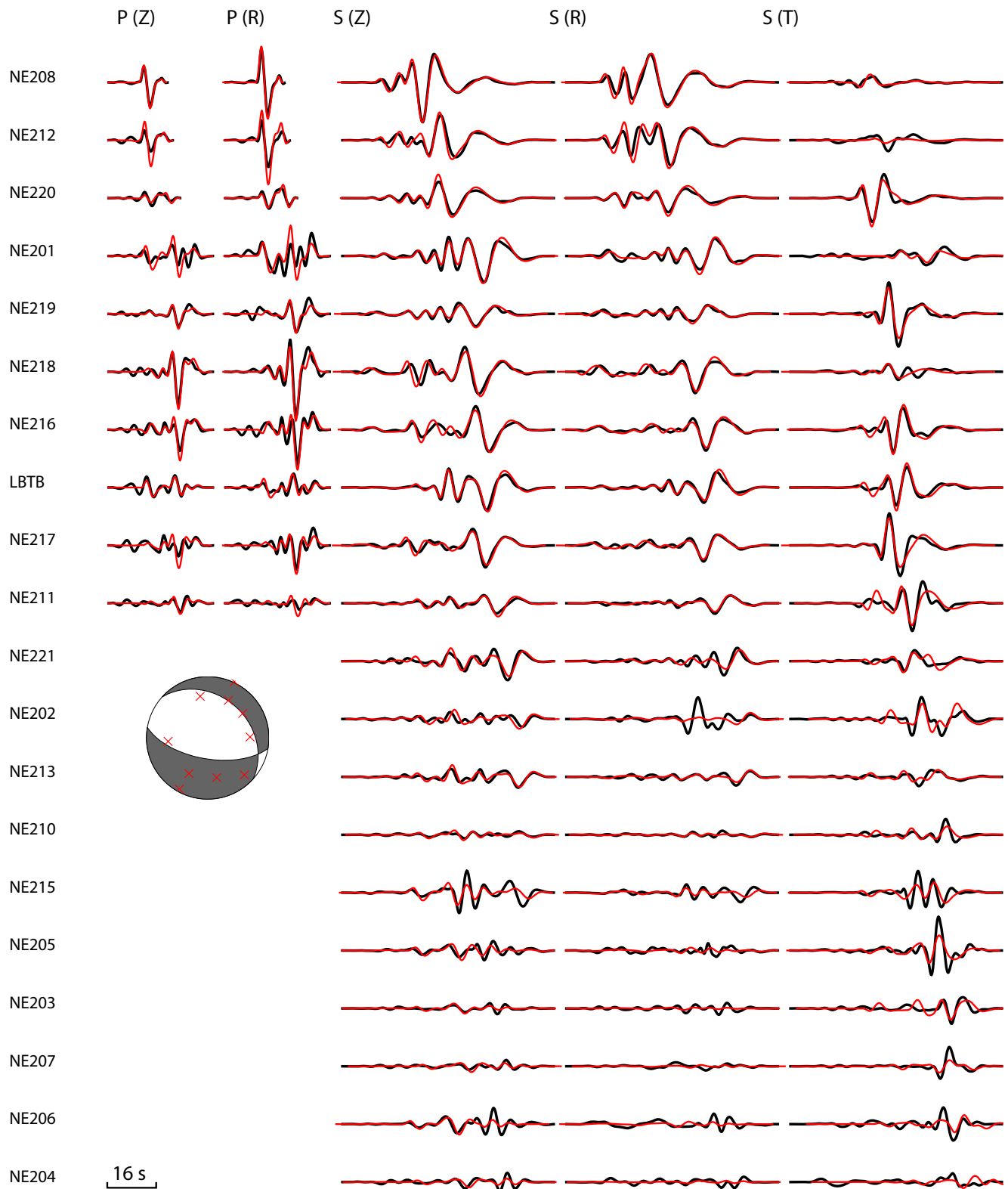
Figure 4. *P* and *S* waveforms of the 2017-07-04 aftershock with *P* waves on the vertical (Z) and radial (R) component, and *S* waves on the vertical, radial and transverse (T) component. Observed data are in black and synthetics in red. Stations are listed with increasing epicentral distance. *P* waves at distances larger than 300 km were excluded because of insufficient signal-to-noise ratio. Red crosses in the focal mechanism indicate azimuth and take-off angle of the *P* waves on the focal sphere.

Figure 5. Focal mechanisms obtained by waveform inversion. Gray lines indicate boundaries between tectonic units and black lines represent known faults.
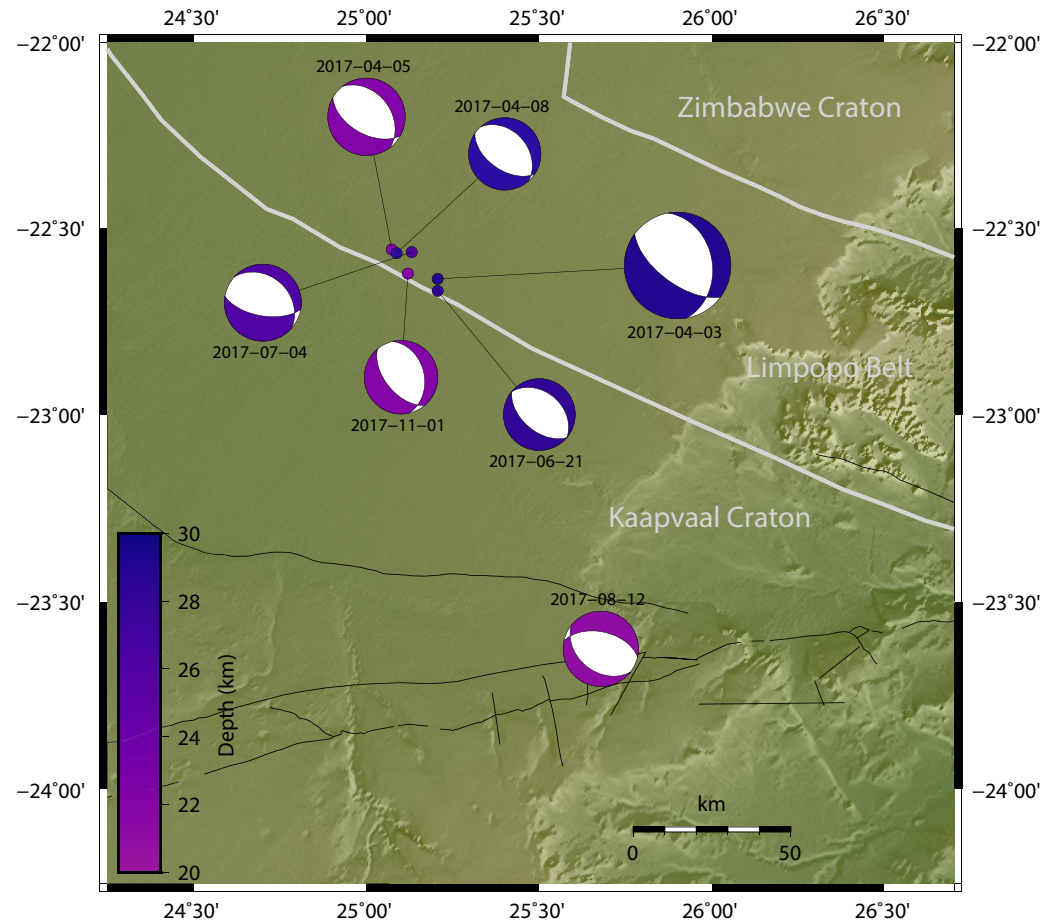
Materna et al., 2019) and suggest an initial stress release during the mainshock at around 30 km followed by triggered aftershocks that occur at shallower depths.

6. Rupture Propagation of Mainshock

We found that the waveforms of the mainshock were less well fit than those of the aftershocks for which modeling by a simple point source was adequate. This suggests that there are effects of rupture propagation in the waveform data of the main event which may be retrieved with the empirical Green's function approach (e.g., Hutchings & Viegas, 2012). In this method a nearby event is selected with a similar moment tensor, but with a size that is at least one magnitude lower. This lower magnitude event has similar radiation and propagation effects, but is better approximated by a point source. A recording of this smaller event is referred to as the empirical Green's function (EGF) for the station considered. Deconvolution of the main event by its EGF yields an estimate of the main event's source-time function (STF) for that station. Similar to the Doppler effect, the STF is shortest when the rupture propagates in the direction of the receiver and is longest when it propagates away from it. From the azimuthal distribution of the STF durations, the rupture direction, its extent in the horizontal plane and the rupture velocity can be estimated (Savage, 1965).

The aftershock on 4 July (2017-07-04, 11:37:06) was selected as the EGF event. A stabilized deconvolution of the vertical component of mainshock by its EGF was performed for a 320 s time window starting from the origin time. After frequency filtering (0.02–0.2 Hz) and rejection of stations with low- or high-frequency artifacts, results of 11 stations could be used to estimate their STF duration (9 NARS-Botswana stations plus two stations operated by the U.S. Geological Survey). Figure 7a shows the deconvolution results. The STF is interpreted as
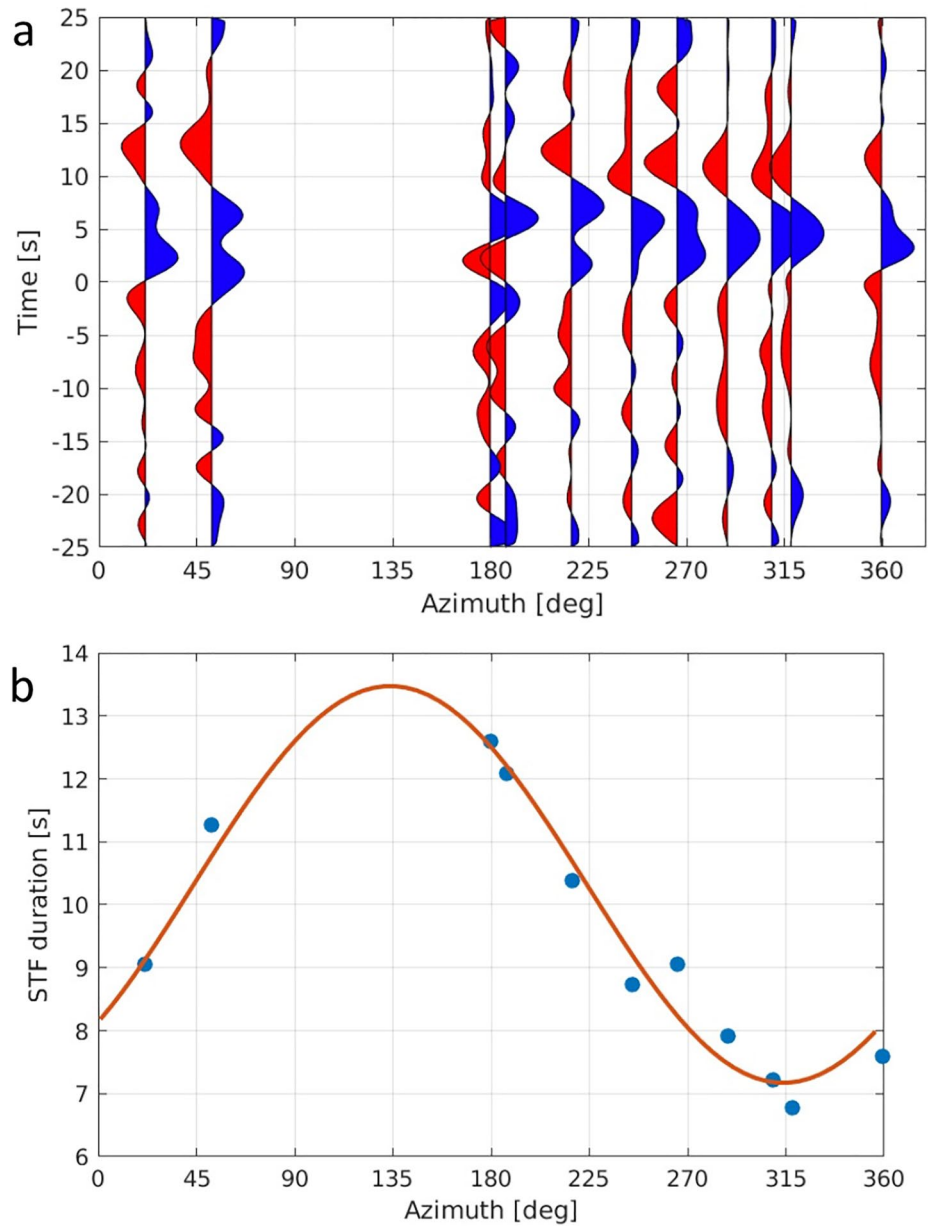
Figure 6. (a) Deconvolution results for stations LSZ, NE217, BOSA, NE221, NE213, NE202, NE211, NE210, NE207, NE204 and NE206 with increasing azimuth. (b) Measurements of source-time function (STF) duration and fit for $L_r = 12.3$ km, $c_r = 2.27$ km/s and $\theta_r = 314°$.

the single or double positive lobe(s) near $t = 0$ s, with the zero crossings taken as the start and stop times. A unidirectional rupture-propagation model gives the following relation between the STF duration (τ) at an azimuth (θ) for a given propagation velocity c

$$\tau = \frac{L_r}{c_r} - \frac{L_r}{c}\cos(\theta - \theta_r) \tag{1}$$

where L_r is the (horizontal) rupture length, c_r the rupture velocity and θ_r the rupture propagation direction. Given that our deconvolutions are filtered between 0.02 and 0.2 Hz, an additional term W is incorporated to account for pulse broadening, resulting in shifts of the start and stop times.

$$\tau = \frac{L_r}{c_r} - \frac{L_r}{c}\cos(\theta - \theta_r) + W \tag{2}$$

Table 1
Earthquake Depth, Moment Magnitude and Focal Mechanism From P and S Waveform Fitting

Date	Origin time	Lat. (°N)	Lon. (°E)	Depth (km)	Mw	NP1	NP2
2017-04-03	17:40:17	−22.636	25.206	29	6.3	350/35/-52	126/63/-113
2017-04-05	00:55:51	−22.557	25.073	22	4.6	322/38/-72	120/54/-104
2017-04-08	19:55:33	−22.567	25.087	21	4.3	319/37/-78	124/54/-99
2017-06-21	07:10:32	−22.668	25.206	28	4.2	310/37/-90	130/53/-90
2017-07-04	11:37:06	−22.564	25.131	26	4.6	312/32/-62	100/62/-106
2017-08-12	02:37:46	−23.626	25.678	21	4.6	283/53/-106	128/40/-70
2017-11-01	12:12:41	−22.622	25.120	22	4.3	347/37/-68	140/56/-106

Note. NP1 and NP2 are the two nodal planes given as strike/dip/rake in degrees. Event date, origin time and epicentral location are taken from the NARS-Botswana event catalog (Section 3).

We estimate the pulse width W caused by the band pass filter to be 4.9 s (Figure 7a). With a lower crustal shear wave speed c of 3.9 km/s at the source depth of 29 km (Fadel et al., 2020), the following parameters were fitted: $L_r = 12.3$ km, $c_r = 2.27$ km/s, $\theta_r = 314°$ (wih an RMS error of 0.295 s). We note that the values of L_r and c_r are strongly dependent on c but that θ_r is tightly constrained by the good azimuthal station coverage. The rupture propagation direction (to the northwest) agrees with the boundary between the Limpopo Belt and the Kaapvaal Craton, the distribution of the aftershocks (all northwest of the mainshock), as well as the strike of the nodal planes of the main event and the aftershocks.

7. Discussion

Events of the 2014–2018 NARS-Botswana catalog (Figure 2) demonstrate that Botswana seismicity does not predominantly occur in the Okavango Rift Zone, but appears to be wider spread. In particular, the 3 April 2017, mainshock and its aftershocks indicate the presence of a seismically active zone around the southern boundary of the Limpopo Belt with the Kaapvaal Craton, a region that was unknown to be active before 2017.
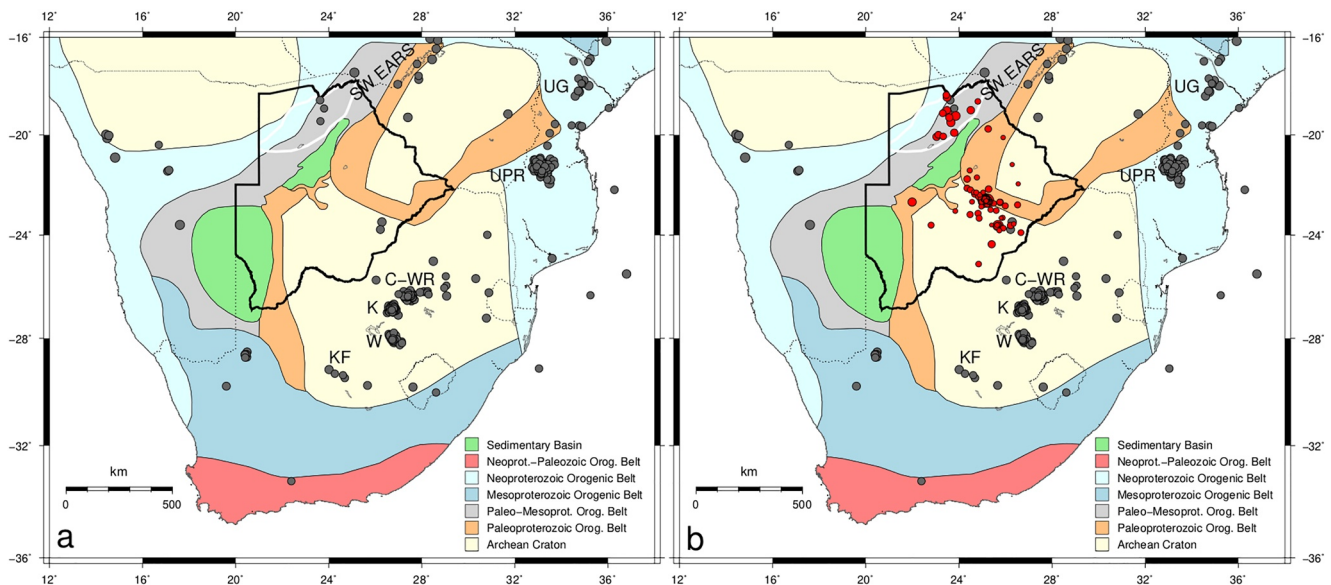
Figure 7. (a) Events with $m_b \geq 4$ in the period 1990–2016 from the reviewed ISC catalog. (b) Events from the NARS-Botswana catalog (2014 - Feb. 2018) added in red. Tectonic features: SW-EARS = Southwestern branch of East African Rift System, UG = Urema Graben, UPR = Urrongas protorift. Mining districts in South Africa (from Singh et al., 2009): C-WR = Carletonville-West Rand, K = Klerksdorp, W = Welkom, KF = Koffiefontein. Note that many events in South Africa are related to mining.

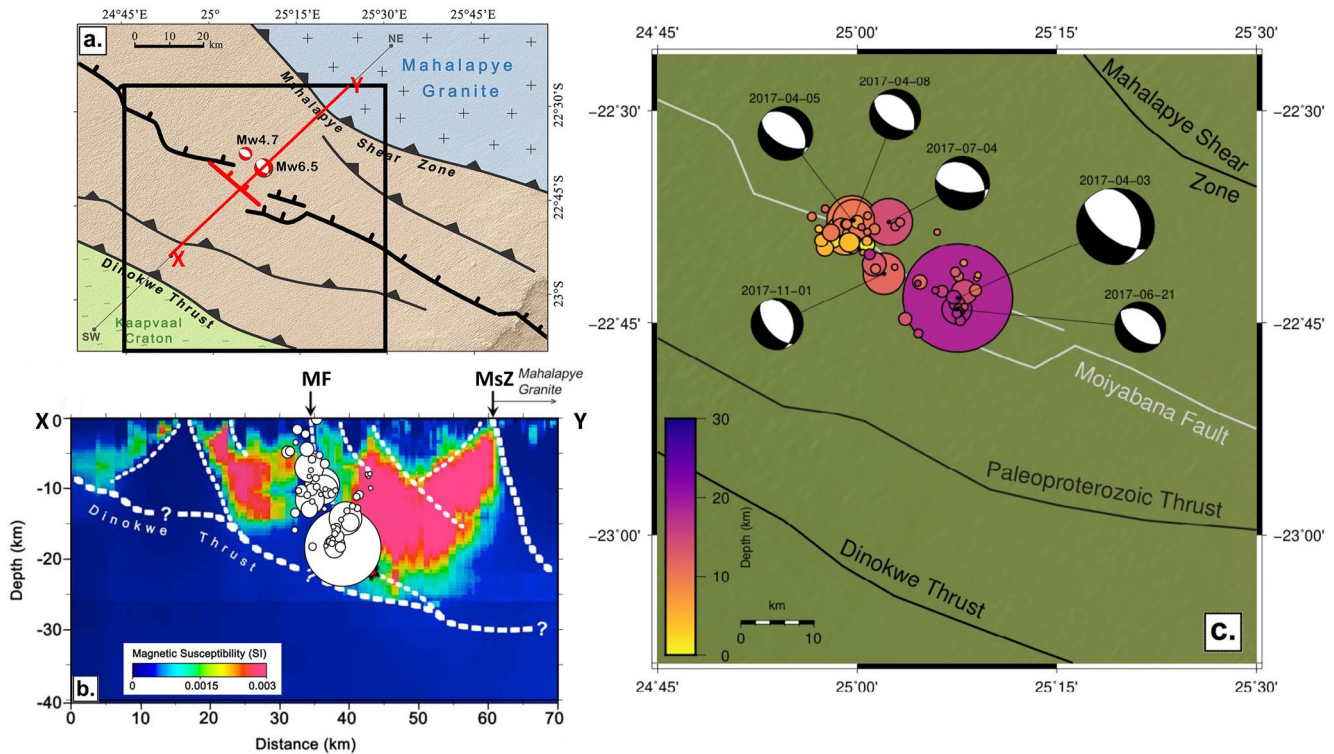**Figure 8.** (a and b) adapted from Kolawole et al. (2017): (a) Interpretation of the tectonic setting. (b) Cross-section through 3-D model inverted from aeromagnetic data with interpreted faults. The relocated events from Figure 3c are plotted on top. (c) Map of relocated events and focal mechanisms within the box indicated in (a).

To put this observation in a wider perspective, we show the events of the reviewed ISC catalog for the period 1990–2016 with $m_b \geq 4$ in Figure 4a. Prior to 1990, station coverage in southern Africa was very poor, and the time span also excludes the seismicity related to the 2017 mainshock. The (somewhat large) minimum magnitude limit was taken to eliminate most of the mining related events, although four regions with mining induced events in South Africa can still be recognized. The figure illustrates that Botswana is a country of low seismic activity with only five events with $m_b \geq 4$ in the 27 years time span. Three of them were in the Okavango Rift Zone (ORZ) and are related to the continuation of the southwestern branch of the East African Rift System (EARS). The other two events in the northern Kaapvaal Craton occurred along the Zoetfontein Fault.

The natural seismicity of our Botswana catalog is added in Figure 4b (events located in mining regions were discarded from our catalog). Although most of the events have magnitudes smaller than 4, their distribution seems to fill the region between the seismicity of the Okavango Rift Zone in the north and that of the Zoetfontein Fault in the northern part of the Kaapvaal Craton. This zone, with many events around the tectonic boundary between the Kaapvaal Craton and the Limpopo Belt, is mostly related to the 3 April 2017, mainshock and its aftershocks, but it also includes two events prior to the mainshock (in 2014 and 2015). The zone is not recognized in any previous maps of Botswana seismicity.

Double-difference relocation of the 3 April 2017, aftershocks resulted in a narrow distribution with a northwesterly orientation dipping toward the northeast (Figures 3 and 8c). There is no direct evidence for the presence of faults in this region because the Precambrian basement is overlain by a thick cover of Kalahari sands. The association of the mainshock and aftershocks to potential faults therefore relies on the interpretation of aeromagnetic and gravity data. The mainshock is located in the Southern Marginal Zone of the Limpopo Belt as inferred from gravity data (Kolawole et al., 2017; Ranganai et al., 2002). This zone is bounded by the Dinokwe Thrust in the southwest and the Mahalapye Shear Zone in the northeast (Figure 8a) and was formed during the Paleoproterozoic collision of the Kaapvaal and Zimbabwe cratons (Ranganai et al., 2002). Kolawole et al. (2017) analyzed and inverted aeromagnetic data and found that the hypocenter of the mainshock coincided with a faultlike feature in their model, which they named the Moiyabana Fault. Figure 8b presents a cross-section from their paper with our relocated events plotted on top. It shows that the mainshock and most of the aftershocks follow the Moiyabana

Fault, confirming the interpretation by Kolawole et al. (2017). Nevertheless, it should be noted that the depth distribution by double-difference relocation is biased by the original event depths, most of which were fixed at 10 km which is too shallow for many of the lower crustal events (Table 1). The actual distribution is therefore likely to be deeper. Moreover, the depth resolution of aeromagnetic inversions is also limited. This means that the lateral locations of the features shown in Figure 8b are better constrained than their vertical positions. The figure further shows that not all the aftershocks follow the interpreted Moiyabana Fault, there is an additional faint branch of low magnitude events with an opposite dip that delineates a potential antithetic fault. This interpretation is strengthened by the aeromagnetic model because this branch approximately outlines the southwestern boundary of a body of high magnetic susceptibility. Thus, the relocated aftershock distribution not only confirms the presence of the Moiyabana Fault but also suggests a more complex fault system than previously inferred from gravity and aeromagnetic data.

We compared the depths of the main- and aftershocks obtained by double difference relocation to those that were obtained by waveform fitting (Table 1) and found them to be consistently 10–12 km shallower. As stated previously, such a shift is expected for events that occurred in the lower crust but were given a fixed depth of 10 km as input for the double difference inversion because the inversion keeps the centroid location of the earthquake cluster fixed. It suggests that the double difference depths of all events are roughly 11 km shallower compared to their more reliably estimated waveform depths.

The focal mechanisms of the waveform-fitted events are also consistent with the Moiyabana Fault. The nodal planes with strikes between 310° and 350° not only match the general strike of this fault, their dips between 32° and 38° toward the northeast also agree with the dip of the Moiyabana Fault in the lower part of the crust (Figure 8b).

The EGF analysis of the mainshock yielded a rupture propagation direction toward the northwest ($\theta_r = 314°$). This direction not only matches the strike of the Moiyabana Fault, it is also consistent with the distribution of aftershocks that mostly occurred northwest of the main event. The rupture propagation direction and the aftershock distribution both suggest that faulting progressed toward the northwest, not only for the main event, but also for the aftershocks.

The focal mechanisms of the events obtained by waveform modeling are all of normal faulting type with a NW-SE strike (Figure 6), indicative of NE-SW extension. This extension direction is consistent with the no-net rotation absolute plate motion direction (Argus et al., 2011; Gripp & Gordon, 1990; Wang et al., 2018). In addition, it is consistent with the NE-SW fast polarization directions obtained from shear wave splitting data (Yu et al., 2015) and surface wave data with asthenospheric sensitivity (Adam & Lebedev, 2012). It is therefore tempting to relate the focal mechanisms to a large scale NE-SW extensional crustal stress regime caused by mantle flow and coupling between the mantle and crust. However, such an interpretation is inconsistent with focal mechanism orientations on a larger scale, because they change from normal faulting with a NW-SE strike in central Botswana (this study) to normal faulting with a NE-SW strike in the ORZ (e.g., Bird et al., 2006). This 90° change in orientation over a distance of 300 km is not easily explained by a large-scale stress field in the crust. Instead, we observe that the strikes of the focal mechanisms, in the ORZ as well as those in central Botswana, match the orientations of their fault systems. It implies that local conditions and structural features largely determine the orientations of the focal mechanisms.

The question that then remains is: What caused the central Botswana earthquakes? Global studies on crustal earthquakes in intraplate settings often invoke fluid transport along existing faults (Calais et al., 2016; Mooney et al., 2012), and several studies have shown that fluids or melt indeed play an important role explaining the seismicity along various segments of the EARS (Ebinger et al., 2017; Lee et al., 2017; Lindenfeld et al., 2012; Oliva et al., 2019). Whereas these segments of the EARS are all seismically active and often volcanic in nature, the mainshock in central Botswana occurred in an area without any previously known seismicity. Moreover, it occurred in the lower crust at a depth of 29 km, which is considered to be too deep for brittle failure (W.-P. Chen & Molnar, 1983). Yet, lower crustal earthquakes are not uncommon in cratonic areas of the EARS (Craig et al., 2011; Yang & Chen, 2010). The occurrence of lower crustal earthquakes has been explained by fluid-induced eclogitization, that is transformational faulting caused by the breakdown of a dry metastable granulite facies rock to eclogite (Jackson et al., 2004). In recent years there is growing evidence that supports this mechanism based on observations on exposed rocks (Austrheim, 1987; John & Schenk, 2003, 2006; Petley-Ragan et al., 2019),

laboratory experiments (Incel et al., 2019), petrological and geophysical modeling (Henry et al., 1997; Hetényi et al., 2021; Malvoisin et al., 2020) and seismic studies (Michailos et al., 2021; Priestley et al., 2008). It can be a top-down process (Jamtveit et al., 2018, 2016; Moecher & Steltenpohl, 2009), but in central Botswana it was a bottom-up process with lower crustal initiation of the mainshock at 29 km depth, and upward migration of the aftershocks in a northwesterly direction.

Eclogitization of the lower crust, as suggested here, requires fluid infiltration to initiate the mainshock by a chemical reaction, where a tiny amount of fluid is sufficient to start the process (Incel et al., 2019; Jackson et al., 2004). The transformation to eclogite will lead to a loss in strength and is accompanied by an increase in porosity and permeability caused by the volume reduction. This allows the fluids to infiltrate further, and the process is repeated, creating sequential aftershocks. Moorkamp et al. (2019) were unable to detect a mantle source of fluids in their seismic and resistivity models, but the more detailed tomographic study by Fadel et al. (2020) using NARS-Botswana data revealed a thin low shear-velocity anomaly in the uppermost mantle that links the main event to a large strong low velocity anomaly in the mantle beneath the eastern ORZ (see their Figure 4). This low velocity anomaly in the uppermost mantle may be interpreted as the mantle source of fluids. The low velocity anomaly beneath the ORZ was also found in several other (lower resolution) tomographic P and S wave velocity models (Ortiz et al., 2019; White-Gaynor et al., 2020), and may be related to decompression melting caused by lithospheric thinning in response to tensional stresses (Yu et al., 2017). The normal-faulting focal mechanisms are consistent with the tensional stress regime that is required for such a scenario.

The earthquakes in central Botswana suggest that the Kalahari Craton, formed by the amalgamation of the Kaapvaal Craton, Limpopo Belt and Zimbabwe Craton during Paleoproterozoic collision (2.7–2.6 Ga), has started to break up along one of its ancient suture zones. How this will develop in the future is unclear. It is generally believed that the African superplume plays an important role in rifting the African continent (Forte et al., 2010; Koptev et al., 2016). Nevertheless, geodynamic studies agree that lithospheric stresses arising from mantle coupling and lithospheric buoyancy forces are insufficient to initiate rifting (Ghosh & Holt, 2012; Stamps et al., 2018) and that pre-existing weak zones are needed for rifting to occur (Celli et al., 2020; Kendall & Lithgow-Bertelloni, 2016; Stamps et al., 2018). The earthquakes in central Botswana investigated in this study suggest that the southern margin of the Limpopo Belt is such a zone that is currently weakened by upward fluid transport from the mantle. The earthquake distribution of our catalog further suggests that the southwestern branch of the EARS may continue from the ORZ southwards along the southern boundary of the Limpopo Belt with the Kaapvaal Craton, in agreement with the hypothesis by Malservisi et al. (2013) based on geodetic data.

8. Conclusion

The deployment of 21 seismic stations of the NARS-Botswana network (2013–2018) allowed several seismic studies that provide new insights into the seismotectonics of the region. We created a new 4-year catalog of seismic events with an estimated magnitude of completeness of 3.1. The catalog confirms the seismic activity of the Okavango Rift Zone, which is currently interpreted as the terminus of the southwestern branch of the East African Rift System. In addition, the catalog lists the events in central Botswana that are related to the unexpected Mw 6.5 earthquake of 3 April 2017. Double-difference relocation of the aftershocks of this main event shows that a fault zone along the southern margin of the Limpopo Belt is reactivated. This fault system, formed as a thrust system during Paleoproterozoic collision of the Kaapvaal and Zimbabwe cratons (2.7–2.6 Ga), is now reactivated within a tensional stress regime as is evident from the focal mechanisms. The initiation of the mainshock at a lower crustal depth of 29 km with rupture propagation to the northwest along the Moiyabana Fault, together with the upward migration of the aftershocks along its fault system, points to eclogitization of a dry metastable granulite facies rock triggered by fluid infiltration. The presence of a low velocity anomaly in the uppermost mantle (Fadel et al., 2020) provides additional support for this scenario. Whereas fluid transport has previously been suggested for earthquake occurrence in stable continental regions (Craig et al., 2011), this is, to our knowledge, the first study that interprets eclogitization in the lower crust from a main- and aftershock distribution. Furthermore, we speculate that rifting in the Okavango Rift Zone will continue southwards along the southern boundary of the Limpopo Belt, thus extending the southwestern branch of the East African Rift Zone into central Botswana. New data from the Botswana Seismic Network may help to resolve this hypothesis.

Data Availability Statement

The data used in this study are available from the IRIS Data Management Center: http://service.iris.edu/fdsnws/dataselect/1/.

References

Adam, J. M.-C., & Lebedev, S. (2012). Azimuthal anisotropy beneath southern Africa from very broad-band surface-wave dispersion measurements. *Geophysical Journal International*, *191*(1), 155–174. https://doi.org/10.1111/j.1365-246x.2012.05583.x

Albano, M., Polcari, M., Bignami, C., Moro, M., Saroli, M., & Stramondo, S. (2017). Did anthropogenic activities trigger the 3 April 2017 Mw 6.5 Botswana earthquake? *Remote Sensing*, *9*(10), 1028. https://doi.org/10.3390/rs9101028

Argus, D. F., Gordon, R. G., & DeMets, C. (2011). Geologically current motion of 56 plates relative to the no-net-rotation reference frame. *Geochemistry, Geophysics, Geosystems*, *12*(11), Q11001. https://doi.org/10.1029/2011gc003751

Austrheim, H. (1987). Eclogitization of lower crustal granulites by fluid migration through shear zones. *Earth and Planetary Science Letters*, *81*(2–3), 221–232. https://doi.org/10.1016/0012-821x(87)90158-0

Begg, G., Griffin, W., Natapov, L., O'Reilly, S. Y., Grand, S., O'Neill, C., et al. (2009). The lithospheric architecture of Africa: Seismic tomography, mantle petrology, and tectonic evolution. *Geosphere*, *5*(1), 23–50. https://doi.org/10.1130/ges00179.1

Bird, P., Ben-Avraham, Z., Schubert, G., Andreoli, M., & Viola, G. (2006). Patterns of stress and strain rate in southern Africa. *Journal of Geophysical Research*, *111*(B8), B08402. https://doi.org/10.1029/2005jb003882

Bouwman, D. (2019). *Relocating aftershocks of the 2017 Moiyabana, Botswana earthquake* (MSc thesis). Utrecht University. Retrieved from https://seismologie.sites.uu.nl/research-projects/nars/botswana/

Bufford, K. M., Atekwana, E. A., Abdelsalam, M. G., Shemang, E., Atekwana, E. A., Mickus, K., et al. (2012). Geometry and faults tectonic activity of the Okavango Rift Zone, Botswana: Evidence from magnetotelluric and electrical resistivity tomography imaging. *Journal of African Earth Sciences*, *65*, 61–71. https://doi.org/10.1016/j.jafrearsci.2012.01.004

Calais, E., Camelbeeck, T., Stein, S., Liu, M., & Craig, T. (2016). A new paradigm for large earthquakes in stable continental plate interiors. *Geophysical Research Letters*, *43*(20), 10–621. https://doi.org/10.1002/2016gl070815

Celli, N. L., Lebedev, S., Schaeffer, A. J., & Gaina, C. (2020). African cratonic lithosphere carved by mantle plumes. *Nature Communications*, *11*(1), 1–10. https://doi.org/10.1038/s41467-019-13871-2

Chen, W., Ni, S., Kanamori, H., Wei, S., Jia, Z., & Zhu, L. (2015). CAPjoint, a computer software package for joint inversion of moderate earthquake source parameters with local and teleseismic waveforms. *Seismological Research Letters*, *86*(2A), 432–441. https://doi.org/10.1785/0220140167

Chen, W.-P., & Molnar, P. (1983). Focal depths of intracontinental and intraplate earthquakes and their implications for the thermal and mechanical properties of the lithosphere. *Journal of Geophysical Research*, *88*(B5), 4183–4214. https://doi.org/10.1029/jb088ib05p04183

Chisenga, C., Van der Meijde, M., Yan, J., Fadel, I., Atekwana, E. A., Steffen, R., & Ramotoroko, C. (2020). Gravity derived crustal thickness model of Botswana: Its implication for the Mw 6.5 April 3, 2017, Botswana earthquake. *Tectonophysics*, *787*, 228479. https://doi.org/10.1016/j.tecto.2020.228479

Craig, T., Jackson, J., Priestley, K., & McKenzie, D. (2011). Earthquake distribution patterns in Africa: Their relationship to variations in lithospheric and geological structure, and their rheological implications. *Geophysical Journal International*, *185*(1), 403–434. https://doi.org/10.1111/j.1365-246x.2011.04950.x

Ebinger, C. J., Keir, D., Bastow, I. D., Whaler, K., Hammond, J. O., Ayele, A., et al. (2017). Crustal structure of active deformation zones in Africa: Implications for global crustal processes. *Tectonics*, *36*(12), 3298–3332. https://doi.org/10.1002/2017tc004526

Fadel, I., Paulssen, H., van der Meijde, M., Kwadiba, M., Ntibinyane, O., Nyblade, A., & Durrheim, R. (2020). Crustal and upper mantle shear wave velocity structure of Botswana: The 3 April 2017 central Botswana earthquake linked to the East African Rift System. *Geophysical Research Letters*, *47*(4), e2019GL085598. https://doi.org/10.1029/2019gl085598

Fadel, I., van der Meijde, M., & Paulssen, H. (2018). Crustal structure and dynamics of Botswana. *Journal of Geophysical Research: Solid Earth*, *123*(12), 10659–10671. https://doi.org/10.1029/2018jb016190

Forte, A. M., Quéré, S., Moucha, R., Simmons, N. A., Grand, S. P., Mitrovica, J. X., & Rowley, D. B. (2010). Joint seismic–geodynamic-mineral physical modelling of African geodynamics: A reconciliation of deep-mantle convection with surface geophysical constraints. *Earth and Planetary Science Letters*, *295*(3–4), 329–341. https://doi.org/10.1016/j.epsl.2010.03.017

Gardonio, B., Jolivet, R., Calais, E., & Leclère, H. (2018). The April 2017 Mw 6.5 Botswana earthquake: An intraplate event triggered by deep fluids. *Geophysical Research Letters*, *45*(17), 8886–8896. https://doi.org/10.1029/2018gl078297

GFZ (2008). *The SeisComP seismological software package*. GFZ Data Services, GFZ German Research Centre for Geosciences and gempa GmbH. https://doi.org/10.5880/GFZ.2.4.2020.003

Ghosh, A., & Holt, W. E. (2012). Plate motions and stresses from global dynamic models. *Science*, *335*(6070), 838–843. https://doi.org/10.1126/science.1214209

Gripp, A. E., & Gordon, R. G. (1990). Current plate velocities relative to the hotspots incorporating the NUVEL-1 global plate motion model. *Geophysical Research Letters*, *17*(8), 1109–1112. https://doi.org/10.1029/gl017i008p01109

Henry, P., Le Pichon, X., & Goffé, B. (1997). Kinematic, thermal and petrological model of the Himalayas: Constraints related to metamorphism within the underthrust Indian crust and topographic elevation. *Tectonophysics*, *273*(1–2), 31–56. https://doi.org/10.1016/s0040-1951(96)00287-9

Hetényi, G., Chanard, K., Baumgartner, L. P., & Herman, F. (2021). Metamorphic transformation rate over large spatial and temporal scales constrained by geophysical data and coupled modelling. *Journal of Metamorphic Geology*, *39*(9), 1131–1143. https://doi.org/10.1111/jmg.12604

Hutchings, L., & Viegas, G. (2012). Application of empirical Green's functions in earthquake source, wave propagation and strong ground motion studies. *Earthquake Research and Analysis-New Frontiers in Seismology*, 87–140. https://doi.org/10.5772/28189

Incel, S., Labrousse, L., Hilairet, N., John, T., Gasc, J., Shi, F., et al. (2019). Reaction-induced embrittlement of the lower continental crust. *Geology*, *47*(3), 235–238. https://doi.org/10.1130/g45527.1

ISC. (2018). *On-line bulletin*. https://doi.org/10.31905/D808B830

Jackson, J., Austrheim, H., McKenzie, D., & Priestley, K. (2004). Metastability, mechanical strength, and the support of mountain belts. *Geology*, *32*(7), 625–628. https://doi.org/10.1130/g20397.1

Jamtveit, B., Austrheim, H., & Putnis, A. (2016). Disequilibrium metamorphism of stressed lithosphere. *Earth-Science Reviews*, *154*, 1–13. https://doi.org/10.1016/j.earscirev.2015.12.002

Jamtveit, B., Ben-Zion, Y., Renard, F., & Austrheim, H. (2018). Earthquake-induced transformation of the lower crust. *Nature*, *556*(7702), 487–491. https://doi.org/10.1038/s41586-018-0045-y

John, T., & Schenk, V. (2003). Partial eclogitisation of gabbroic rocks in a late Precambrian subduction zone (Zambia): Prograde metamorphism triggered by fluid infiltration. *Contributions to Mineralogy and Petrology*, *146*(2), 174–191. https://doi.org/10.1007/s00410-003-0492-8

John, T., & Schenk, V. (2006). Interrelations between intermediate-depth earthquakes and fluid flow within subducting oceanic plates: Constraints from eclogite facies pseudotachylytes. *Geology*, *34*(7), 557–560. https://doi.org/10.1130/g22411.1

Kendall, J.-M., & Lithgow-Bertelloni, C. (2016). Why is Africa rifting? *Geological Society, London, Special Publications*, *420*(1), 11–30. https://doi.org/10.1144/sp420.17

Kennett, B., & Engdahl, E. (1991). Traveltimes for global earthquake location and phase identification. *Geophysical Journal International*, *105*(2), 429–465. https://doi.org/10.1111/j.1365-246x.1991.tb06724.x

Key, R. M., & Ayres, N. (2000). The 1998 edition of the national geological map of Botswana. *Journal of African Earth Sciences*, *30*(3), 427–451. https://doi.org/10.1016/s0899-5362(00)00030-0

Kinabo, B. D., Atekwana, E. A., Hogan, J. P., Modisi, M. P., Wheaton, D. D., & Kampunzu, A. (2007). Early structural development of the Okavango Rift Zone, NW Botswana. *Journal of African Earth Sciences*, *48*(2–3), 125–136. https://doi.org/10.1016/j.jafrearsci.2007.02.005

Kolawole, F., Atekwana, E. A., Malloy, S., Stamps, D. S., Grandin, R., Abdelsalam, M. G., et al. (2017). Aeromagnetic, gravity, and differential interferometric synthetic aperture radar analyses reveal the causative fault of the 3 April 2017 Mw 6.5 Moiyabana, Botswana, earthquake. *Geophysical Research Letters*, *44*(17), 8837–8846. https://doi.org/10.1002/2017gl074620

Koptev, A., Burov, E., Calais, E., Leroy, S., Gerya, T., Guillou-Frottier, L., & Cloetingh, S. (2016). Contrasted continental rifting via plume-craton interaction: Applications to central East African Rift. *Geoscience Frontiers*, *7*(2), 221–236. https://doi.org/10.1016/j.gsf.2015.11.002

Lee, H., Fischer, T. P., Muirhead, J. D., Ebinger, C. J., Kattenhorn, S. A., Sharp, Z. D., et al. (2017). Incipient rifting accompanied by the release of subcontinental lithospheric mantle volatiles in the Magadi and Natron basin, East Africa. *Journal of Volcanology and Geothermal Research*, *346*, 118–133. https://doi.org/10.1016/j.jvolgeores.2017.03.017

Leseane, K., Atekwana, E. A., Mickus, K. L., Abdelsalam, M. G., Shemang, E. M., & Atekwana, E. A. (2015). Thermal perturbations beneath the incipient Okavango Rift Zone, northwest Botswana. *Journal of Geophysical Research: Solid Earth*, *120*(2), 1210–1228. https://doi.org/10.1002/2014jb011029

Lindenfeld, M., Rümpker, G., Link, K., Koehn, D., & Batte, A. (2012). Fluid-triggered earthquake swarms in the Rwenzori region, East African Rift—Evidence for rift initiation. *Tectonophysics*, *566*, 95–104. https://doi.org/10.1016/j.tecto.2012.07.010

Malservisi, R., Hugentobler, U., Wonnacott, R., & Hackl, M. (2013). How rigid is a rigid plate? Geodetic constraint from the TrigNet CGPS network, South Africa. *Geophysical Journal International*, *192*(3), 918–928. https://doi.org/10.1093/gji/ggs081

Malvoisin, B., Austrheim, H., Hetényi, G., Reynes, J., Hermann, J., Baumgartner, L. P., & Podladchikov, Y. Y. (2020). Sustainable densification of the deep crust. *Geology*, *48*(7), 673–677. https://doi.org/10.1130/g47201.1

Materna, K., Wei, S., Wang, X., Heng, L., Wang, T., Chen, W., et al. (2019). Source characteristics of the 2017 Mw6.4 Moijabana, Botswana earthquake, a rare lower-crustal event within an ancient zone of weakness. *Earth and Planetary Science Letters*, *506*, 348–359. https://doi.org/10.1016/j.epsl.2018.11.007

Meghraoui, M., & the IGCP-601 Working Group (2016). The seismotectonic map of Africa. *Episodes*, *39*(1), 9–18. https://doi.org/10.18814/epiiugs/2016/v39i1/89232

Micallef, T. (2019). *Earthquake detection and localisation using the NARS-Botswana data* (MSc thesis). Utrecht University. Retrieved from https://seismologie.sites.uu.nl/research-projects/nars/botswana/

Michailos, K., Carpenter, N. S., & Hetényi, G. (2021). Spatio-temporal evolution of intermediate-depth seismicity beneath the Himalayas: Implications for metamorphism and tectonics. *Frontiers of Earth Science*, *859*. https://doi.org/10.3389/feart.2021.742700

Midzi, V., Saunders, I., Manzunzu, B., Kwadiba, M., Jele, V., Mantsha, R., et al. (2018). The 03 April 2017 Botswana M6.5 earthquake: Preliminary results. *Journal of African Earth Sciences*, *143*, 187–194. https://doi.org/10.1016/j.jafrearsci.2018.03.027

Modisi, M. P., Atekwana, E. A., Kampunzu, A., & Ngwisanyi, T. H. (2000). Rift kinematics during the incipient stages of continental extension: Evidence from the nascent Okavango Rift Basin, northwest Botswana. *Geology*, *28*(10), 939–942. https://doi.org/10.1130/0091-7613(2000)028<0939:rkdtis>2.3.co;2

Moecher, D., & Steltenpohl, M. (2009). Direct calculation of rupture depth for an exhumed paleoseismogenic fault from mylonitic pseudotachylyte. *Geology*, *37*(11), 999–1002. https://doi.org/10.1130/g30166a.1

Mooney, W. D., Ritsema, J., & Hwang, Y. K. (2012). Crustal seismicity and the earthquake catalog maximum moment magnitude (M_{cmax}) in stable continental regions (SCRs): Correlation with the seismic velocity of the lithosphere. *Earth and Planetary Science Letters*, *357*, 78–83. https://doi.org/10.1016/j.epsl.2012.08.032

Moorkamp, M., Fishwick, S., Walker, R. J., & Jones, A. G. (2019). Geophysical evidence for crustal and mantle weak zones controlling intraplate seismicity—The 2017 Botswana earthquake sequence. *Earth and Planetary Science Letters*, *506*, 175–183. https://doi.org/10.1016/j.epsl.2018.10.048

Nthaba, B., Simon, R. E., & Ogubazghi, G. M. (2018). Seismicity study of Botswana from 1966 to 2012. *International Journal of Geosciences*, *9*(12), 707–718. https://doi.org/10.4236/ijg.2018.912043

Oliva, S., Ebinger, C., Wauthier, C., Muirhead, J., Roecker, S., Rivalta, E., & Heimann, S. (2019). Insights into fault-magma interactions in an early-stage continental rift from source mechanisms and correlated volcano-tectonic earthquakes. *Geophysical Research Letters*, *46*(4), 2065–2074. https://doi.org/10.1029/2018gl080866

Ortiz, K., Nyblade, A., van der Meijde, M., Paulssen, H., Kwadiba, M., Ntibinyane, O., et al. (2019). Upper mantle *P* and *S* wave velocity structure of the Kalahari Craton and surrounding Proterozoic terranes, southern Africa. *Geophysical Research Letters*, *46*(16), 9509–9518. https://doi.org/10.1029/2019gl084053

Paige, C. C., & Saunders, M. A. (1982). LSQR: An algorithm for sparse linear equations and sparse least squares. *ACM Transactions on Mathematical Software (TOMS)*, *8*(1), 43–71. https://doi.org/10.1145/355984.355989

Pastier, A.-M., Dauteuil, O., Murray-Hudson, M., Moreau, F., Walpersdorf, A., & Makati, K. (2017). Is the Okavango delta the terminus of the east African Rift system? Towards a new geodynamic model: Geodetic study and geophysical review. *Tectonophysics*, *712*, 469–481. https://doi.org/10.1016/j.tecto.2017.05.035

Petley-Ragan, A., Ben-Zion, Y., Austrheim, H., Ildefonse, B., Renard, F., & Jamtveit, B. (2019). Dynamic earthquake rupture in the lower crust. *Science Advances*, *5*(7), eaaw0913. https://doi.org/10.1126/sciadv.aaw0913

Priestley, K., Jackson, J., & McKenzie, D. (2008). Lithospheric structure and deep earthquakes beneath India, the Himalaya and southern Tibet. *Geophysical Journal International*, *172*(1), 345–362. https://doi.org/10.1111/j.1365-246x.2007.03636.x

Ranganai, R. T., Kampunzu, A., Atekwana, E. A., Paya, B., King, J., Koosimile, D., & Stettler, E. H. (2002). Gravity evidence for a larger Limpopo Belt in southern Africa and geodynamic implications. *Geophysical Journal International*, *149*(3), F9–F14. https://doi.org/10.1046/j.1365-246x.2002.01703.x

Reeves, C. (1972). Rifting in the Kalahari? *Nature*, *237*(5350), 95–96. https://doi.org/10.1038/237095a0

Savage, J. (1965). The effect of rupture velocity upon seismic first motions. *Bulletin of the Seismological Society of America*, *55*(2), 263–275. https://doi.org/10.1785/bssa0550020263

Scholz, C., Koczynski, T., & Hutchins, D. (1976). Evidence for incipient rifting in southern Africa. *Geophysical Journal International*, *44*(1), 135–144. https://doi.org/10.1111/j.1365-246x.1976.tb00278.x

Singh, M., Kijko, A., & Durrheim, R. (2009). Seismotectonic models for South Africa: Synthesis of geoscientific information, problems, and the way forward. *Seismological Research Letters*, *80*(1), 71–80. https://doi.org/10.1785/gssrl.80.1.71

Stamps, D. S., Saria, E., & Kreemer, C. (2018). A geodetic strain rate model for the East African Rift System. *Scientific Reports*, *8*(1), 1–9. https://doi.org/10.1038/s41598-017-19097-w

St-Onge, A. (2011). Akaike information criterion applied to detecting first arrival times on microseismic data. In *SEG technical program expanded abstracts 2011* (pp. 1658–1662). Society of Exploration Geophysicists.

Waldhauser, F., & Ellsworth, W. L. (2000). A double-difference earthquake location algorithm: Method and application to the northern Hayward fault, California. *Bulletin of the Seismological Society of America*, *90*(6), 1353–1368. https://doi.org/10.1785/0120000006

Wang, S., Yu, H., Zhang, Q., & Zhao, Y. (2018). Absolute plate motions relative to deep mantle plumes. *Earth and Planetary Science Letters*, *490*, 88–99. https://doi.org/10.1016/j.epsl.2018.03.021

Wessel, P., Luis, J., Uieda, L., Scharroo, R., Wobbe, F., Smith, W., & Tian, D. (2019). The generic mapping tools version 6. *Geochemistry, Geophysics, Geosystems*, *20*(11), 5556–5564. https://doi.org/10.1029/2019gc008515

White-Gaynor, A., Nyblade, A., Durrheim, R., Raveloson, R., van der Meijde, M., & Fadel, I. (2020). Lithospheric boundaries and upper mantle structure beneath southern Africa imaged by *P* and *S* wave velocity models. *Geochemistry, Geophysics, Geosystems*, *21*(10), e2020GC008925. https://doi.org/10.1029/2020GC008925

White-Gaynor, A., Nyblade, A., Durrheim, R., Raveloson, R., van der Meijde, M., & Fadel, I. (2021). Shear-wave velocity structure of the southern African upper mantle: Implications for Craton structure and plateau uplift. *Geophysical Research Letters*, *48*(7), e2020GL091624. https://doi.org/10.1029/2020GL091624

Wright, J. A., & Hall, J. (1990). Deep seismic profiling in the Nosop Basin, Botswana: Cratons, mobile belts and sedimentary basins. *Tectonophysics*, *173*(1–4), 333–343. https://doi.org/10.1016/0040-1951(90)90228-z

Yang, Z., & Chen, W.-P. (2010). Earthquakes along the East African Rift System: A multiscale, system-wide perspective. *Journal of Geophysical Research*, *115*(B12), B12309. https://doi.org/10.1029/2009jb006779

Yu, Y., Gao, S. S., Moidaki, M., Reed, C. A., & Liu, K. H. (2015). Seismic anisotropy beneath the incipient Okavango Rift: Implications for rifting initiation. *Earth and Planetary Science Letters*, *430*, 1–8. https://doi.org/10.1016/j.epsl.2015.08.009

Yu, Y., Liu, K. H., Huang, Z., Zhao, D., Reed, C. A., Moidaki, M., et al. (2017). Mantle structure beneath the incipient Okavango Rift Zone in southern Africa. *Geosphere*, *13*(1), 102–111. https://doi.org/10.1130/ges01331.1

Zhao, L.-S., & Helmberger, D. V. (1994). Source estimation from broadband regional seismograms. *Bulletin of the Seismological Society of America*, *84*(1), 91–104.

Zhu, L., & Helmberger, D. V. (1996). Advancement in source estimation techniques using broadband regional seismograms. *Bulletin of the Seismological Society of America*, *86*(5), 1634–1641. https://doi.org/10.1785/bssa0860051634